

# Scattering-aware Holographic PIV with Physics-based Motion Priors

Miao Qi and Wolfgang Heidrich, *IEEE Fellow*

**Abstract**—Particle imaging velocimetry is a classical method in 2D fluid imaging. While 3D extensions exist, they are limited by practical restrictions of multi-camera systems. Holographic particle imaging velocimetry has emerged as a solution for a simple and compact 3D imaging system. However, with dense particle seeding, scattering effects become apparent, and the reconstruction quality suffers, especially in the axial direction. To address these challenges, we propose a simple in-line HPIV approach with a plane-to-plane propagation model to account for the scattering effect. Instead of independently reconstructing particle volume and flow velocity, we present a joint optimization problem for particle and flow reconstruction. This optimization problem combines the a differentiable formulation of the holographic image formation with physical motion priors (incompressible flow and particle motion consistency) to improve the reconstruction quality. We solve this joint optimization problem using an extendable automatic differentiation and alternating optimization framework, and we evaluate the proposed method in synthetic and real experiments. The results demonstrate improved reconstruction quality for both particle density and flow velocity fields. With the plane-to-plane propagation model and physics prior, we push HPIV a step further regarding particle density, tank depth, and reconstruction accuracy.

**Index Terms**—Computational Photography, Fluid Imaging, Particle Imaging Velocimetry, Holography

## 1 INTRODUCTION

PARTICLE imaging velocimetry (PIV) [1], [2] is one of the most-used methods for fluid imaging [3], [4], [5], [6], [7], [8], and is widely deployed in diverse fields, such as fluid dynamics, combustion, biology, computer vision, and computer graphics. The technique involves introducing small tracer particles into the flow. The flow velocity field is reconstructed by tracking the motion of these particles using a variety of different algorithms. Basic PIV can only obtain the 2D flow field in a planar slice (2D-2C) [9]. Some extension into 3D include scanning PIV (3D-2C) [10], [11], as well as Stereo-PIV [12], [13] and Tomographic PIV [14] which can reconstruct the full 3D-3C field but requires multiple cameras. Multi-camera setups are often complicated in real fluid experiments due to complex tank geometries or space restrictions.

To enable a single-camera capture setup, holographic particle imaging velocimetry (HPIV) has been proposed [15], [16], [17], [18], [19], [20]. Most previous HPIV methods partition the volume into many slices along the optical path direction and assume that each slice is illuminated by a plane wave and that the perturbed wavefront is directly propagated to the image sensor. In other words, these legacy methods do not model light interactions with other particles either in front of or behind the current plane. As we show in our experiments, this approach degenerates strongly for higher particle densities. This is problematic for fluid imaging since high particle densities are required to resolve small vortices and other features.

As particle density increases, it becomes increasingly

important to inter-slice interaction and the effects of scattering. Recently, a plane-to-plane multi-slice beam propagation method [21], [22], [23], [24], [25], [26] was proposed for cell imaging to account for the scattering effect. This model includes the interaction between slices and accounts for the scattering effects. In this method, the output light field from the previous plane is used as the input light field for the next plane. By using this method, one can account for the scattering effect in holographic reconstruction.

On top of this plane-to-plane transport model, several algorithmic improvements are still possible to improve the reconstruction quality. First, most of the previous methods formed particle reconstruction and flow velocity field reconstruction separately. This pipelined reconstruction approach accumulates errors from one task to another. Second, the legacy methods suffer from a low axial resolution corresponding to a high uncertainty for the  $z$ -coordinates of particle positions. In this work, we show that the physics priors can also be used to increase this axial resolution of the system.

While most previous methods formulate the PIV reconstruction problem as an optimization problem with manually derived analytical gradients, this approach makes it difficult to incorporate more complex image formation models such as the plane-to-plane transport. Here, we show how to combine the *optimization-based* approach that enables the use of physical motion priors with an *automatic differentiation* approach [27] that allows for the use of a complex forward model. In summary, our contributions are:

• Miao Qi and Wolfgang Heidrich are with the Visual Computing Center, King Abdullah University of Science and Technology, Thuwal 23955-6900, Saudi Arabia  
E-mail: miao.qi@kaust.edu.sa; wolfgang.heidrich@kaust.edu.sa;

- we are the first to account for the scattering effect in (Holographic) PIV. We utilize the plane-to-plane multi-slice beam propagation model to simulate the light scattering effect using an automatic differentiation framework;

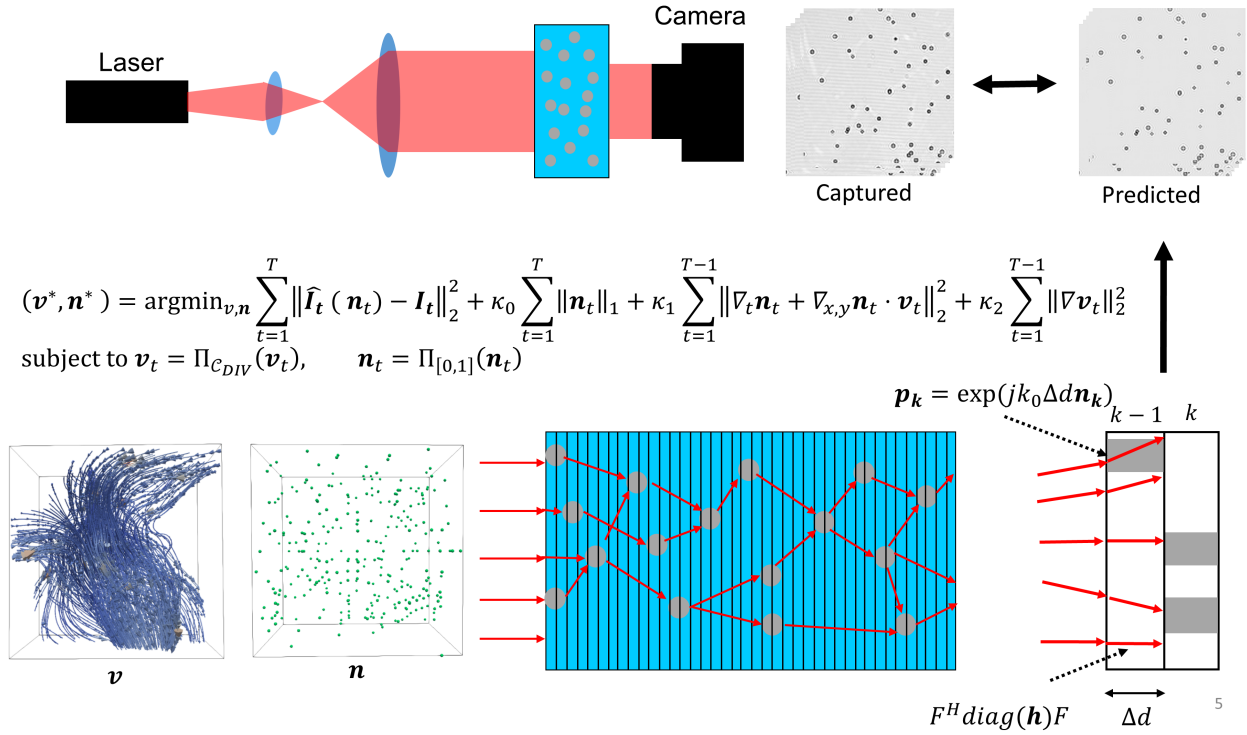


Fig. 1. The proposed approach. Top: Setup based on simple and compact in-line holography. A camera captures multiple frames of holograms. Bottom: Plane-to-plane propagation model. The particle volume frame is discretized into thin slices. For every slice, we simulate the plane-to-plane transport and the complex wave modulation, as depicted on the bottom right. The joint optimization problem, including physical motion priors and divergence-free projection, is presented in the center.

- we combine the new forward model with physical motion priors for the recovered flow field, forming a joint problem for both particle densities and motion fields.

In this study, we conducted ablation experiments on different particle density scenarios, which demonstrate that, as particle density increases, the scattering phenomenon becomes more pronounced and cannot be ignored in high-density particle PIV reconstruction. In the ablation study, we compare the results of plane-to-plane and one-plane-to-last, two different models for different particle densities. We show the effectiveness of the proposed plane-to-plane propagation model. This model can effectively account for scattering effects and significantly improve reconstruction quality for higher-density particle PIV reconstruction.

Furthermore, we conducted additional ablation experiments to assess the efficacy of our proposed motion consistency prior, physical divergence-free prior, and effectiveness of multiple frame measurement in holographic particle imaging velocimetry. Our results showed that with our proposed prior and multiple measurements, we have successfully surpassed the previous limitations in particle density, tank depth, and reconstruction accuracy.

## 2 RELATED WORK

**Particle Image Velocimetry** Particle Image Velocimetry (PIV) is the most widely used method for flow imaging [1], [2]. However, the traditional approach can only measure

the in-plane motion within a slice of the volume (2D-2C). To overcome this limitation, various approaches have been proposed. The Stereo-PIV uses two cameras to obtain the 3D velocity component (2D-3C) [12], [13]. 3D Scanning PIV (SPIV) (3D-2C) [10], [11] uses a fast scanning laser to sweep the light sheet to cover the full reconstruction volume. However, it trades the third dimension for temporal resolution, making it more difficult to image fast flows.

To obtain 3D flows over the full 3D volume (3D-3C), more sophisticated techniques have been proposed, including defocus [28], [29], [30], synthetic aperture PIV [31], tomographic PIV (tomo-PIV) [14], [32], structured-light PIV [33], [34], plenoptic (light field) PIV [35], [36]. Most of the above systems either require multiple cameras or require some special cameras that trade spatial resolution for angular resolution. The setup is not that simple for real fluid experiments with complicated tank geometries. Some systems can achieve the PIV task with a single-camera setup, like Rainbow PIV [33], [37]. Rainbow PIV encodes the depth into color to achieve single-camera 3D-3C PIV, albeit with low-depth resolution.

HPIV [15], [16], [17], [18], [19], [38], [39] has recently emerged as a promising solution to achieving single-camera particle image velocimetry. HPIV utilizes holography to encode depth information, which is represented by the hologram's ring pattern. Only one camera is required. Its setup is remarkably simple and easily implementable. It is demonstrated that particles can be reconstructed very well with the help of prior information. Furthermore, the recon-

struction of flow fields enables the investigation of turbulence dynamics. Chen *et al.* [40] propose a joint optimization approach for flow and particle reconstruction. Our method differs from theirs in two main aspects. Firstly, their method does not account for the scattering effect. They utilize a single-slice-propagate-to-the-last-camera model, which we refer to as the “one2last” model in Section 5.2. In Section 5.2 (Plane2Plane and OnePlane2Last) and supplementary Section 4.3.2, the results demonstrate that, particularly for higher density values, our approach outperforms theirs in terms of flow average absolute error (AAE) and particle localization. The second major distinction lies in the absence of a physical constraint on the flow of their method. In our research, we enhance their approach by incorporating an incompressibility physical prior. This additional constraint contributes to the improved performance of our method, as discussed in Supplement Section 4.3.1.

**Imaging of Scattering Media** The scattering problem would be important in the holographic PIV, especially when the particle density is high. The particle scattering is something that can not be ignored. There are several popular models for scattering medium imaging. The first model is the Lippmann-Schwinger equation. To solve this nonlinear equation, either the Born or the Rytov approximation is used [20], [41], [42], [43], [44]. The primary limitation of this approach is its high cost in terms of both computational time and memory consumption, which restrict its applicability to small-scale problems.

The second method is the multi-slice beam propagation method (BPM). It is memory efficient and can handle relatively large-scale objects. Eckstein *et al.* verify the accuracy of the beam propagation by comparing it with the FDTD full-wave simulation, showing that the BPM is accurate. Lei and Waller propose a multi-slice model [26]. Kamilov *et al.* [21], [22], [23], [24] have a more rigorous analysis of this scattering process and derive the propagation formula from Maxwell equations. The process is accounted for as diffraction and phase delay, with the latter being determined by the difference in refractive index between the object and background medium. The physical explanation for this scattering is attributed to the refractive index discontinuity in the medium. However, their method necessitates the measurement of the complex field, increasing the complexity of the setup. Furthermore, it should be noted that their method is primarily aimed at cell imaging.

Based on this method, Wang *et al.* [25] propose a beam propagation method for particle reconstruction. The authors then combine this image formation model with a sparsity prior to form an optimization problem that is solved with FISTA using manually derived gradients. This approach eliminates the need for a complex field and requires only the intensity image. They also verified the accuracy of the BPM forward simulation result by comparing it with the experimentally captured hologram. Their paper primarily focuses on single-frame particle reconstruction, while our research is centered around HPIV. Although both topics involve the reconstruction of particles, our goals differ significantly. Their study places more emphasis on particle reconstruction, whereas our primary focus lies on flow reconstruction. Regarding the methodology, a key distinction between our paper and theirs is the incorporation of motion consistency

and divergence-free prior in our approach. Additionally, we integrate flow reconstruction into a joint optimization problem, which sets our method apart from theirs. Notably, their method solely utilizes a single-frame hologram as input, whereas our approach can leverage multiple frames to improve the depth resolution of the particle reconstruction.

### 3 SCATTERING HOLOGRAPHIC IMAGING MODEL

The wave equation for the propagation of monochromatic light in a volume is given as:

$$\frac{\partial^2 u}{\partial x^2} + \frac{\partial^2 u}{\partial y^2} + \frac{\partial^2 u}{\partial z^2} + k^2(\mathbf{r})u = 0, \quad (1)$$

$$k(\mathbf{r}) = k_0 n(\mathbf{r}) \quad (2)$$

where  $k(\mathbf{r})$  is the wavenumber of the volume in the tank and  $k_0$  is the wavenumber in the vacuum.  $n(\mathbf{r})$  is a scalar field representing the spatial distribution of the refractive index in the volume. Observing the equation, we can see that the final optical field solution is only related to the refractive index distribution. Assuming that the tank only has liquid and a number of identical particles,  $n(\mathbf{r})$  can be decomposed into two parts:

$$n(\mathbf{r}) = n_0 + \Delta n(\mathbf{r}), \quad (3)$$

where  $n_0$  is the background medium refractive index and  $\Delta n(\mathbf{r})$  is the refractive index perturbation caused by the particle. In our case, the background medium is liquid. For  $\Delta n(\mathbf{r})$ , we assume that all the particles have the same refractive index, so it is just the difference between the particle refractive index and the background liquid refractive index.

The particles in the liquid form an inhomogeneous medium that we can divide into  $N$  very thin slices. Within each slice, the medium is assumed to be homogeneous in the  $z$  direction. We assume that the wave with a slow variation amplitude  $a(\mathbf{r})$  propagates in the  $z$  direction and has the form:

$$u(\mathbf{r}) = a(\mathbf{r}) \exp(jk_0 n_0 z) \quad (4)$$

Within each slice, light propagates and interacts with particles. We have rigorous derivation in the supplement. Intuitively, there are two steps: one is light propagation, and another is the phase delay caused by particle perturbation. After discretization, the whole process can be expressed by the following expression [25]:

$$\mathbf{U}_k(\mathbf{n}) = \text{diag}(\mathbf{p}_k(\mathbf{n}_k)) \mathbf{H}_{\Delta d} \mathbf{U}_{k-1}(\mathbf{n}) \quad (5)$$

Here  $\mathbf{U}_k(\mathbf{n})$  is the light field after the  $k^{th}$  slice, and  $\mathbf{n}$  is the volume refractive index.  $\mathbf{H}_{\Delta d}$  is the operator for propagating by a distance  $\Delta d$  within slice  $k$ . In the Fourier domain, it can be written as  $\mathbf{H}_{\Delta d} = \mathbf{F}^H \text{diag}(\mathbf{h}) \mathbf{F}$ . The  $\mathbf{F}^H$  and  $\mathbf{F}$  are the Fourier transform and inverse Fourier transform, respectively.  $\cdot^H$  is the conjugate transpose. The  $\text{diag}(\mathbf{h})$  is a diagonal matrix formed by the vector  $\mathbf{h}$ . It implements element-wise operations on every slice.  $\mathbf{h}$  is the propagation kernel.

$$\mathbf{h} = \exp[j\Delta d(\sqrt{k_0^2 n_0^2 - \mathbf{k}_x^2 - \mathbf{k}_y^2} - k_0 n_0)], \quad (6)$$

where  $\mathbf{k}_x$  and  $\mathbf{k}_y$  are the spatial frequency component in the  $x$  and  $y$  direction. A rigorous derivation of this formula can be found in the supplement. Note that the term inside the parenthesis is just the angular spectrum kernel minus  $k_0 n_0$ . Phase is a relative term; a constant phase delay does not change the amplitude distribution. When  $\mathbf{k}_x$  and  $\mathbf{k}_y$  are zero, which means there is no perturbation in the medium, and the phase term will not change. This makes sense because if parallel light propagates in a homogeneous, uniform medium, it will not change the amplitude distribution.  $\text{diag}(\mathbf{p}_k(\mathbf{n}_k))$  is the phase delay for every pixel. Its kernel can be expressed in the following form:

$$\mathbf{p}_k(\mathbf{n}_k) = \exp(jk_0 \Delta d \mathbf{n}_k) \quad (7)$$

Here the  $\mathbf{n}_k$  is the refractive index distribution in the  $k^{th}$  slice.

After the last slice, the exit field propagates in free space by a distance  $d_{cam}$  to the camera sensor. The intensity is our predicted hologram  $\hat{\mathbf{I}}$ . This part may have relatively long free space propagation. We choose the angular spectrum propagation kernel [45] for the kernel in  $\mathbf{H}'_{d_{cam}}$ .

$$\hat{\mathbf{I}} = |\mathbf{H}'_{d_{cam}} \mathbf{U}_{\mathbf{N}}(\mathbf{n})|^2 \quad (8)$$

The above is the forward simulation process. The corresponding inverse problem is used for reconstructing the particle volume from the captured hologram. Due to the complexity of the model, no closed-form solution is available for this problem. Instead, we formulate the inverse problem as a joint optimization problem, where the optimization objective is to minimize the discrepancy between the captured hologram and the simulated hologram of the reconstructed particle volume. To this end, we incorporate physical incompressible prior and motion consistency prior into the optimization process. These priors enable us to regularize the optimization process and improve the accuracy of the reconstructed particle volume. And we solve this optimization problem with Automatic Differentiation (AD) and an alternative optimization framework. In the following section, we provide a detailed description of the proposed methodology.

### 3.1 Discussion

We would like to highlight that the refractive index of our particles is 1.59, while the refractive index of the background liquid is 1.33. Additionally, our particle diameter is about 40  $\mu\text{m}$ , and the wavelength of the incident light is 0.6  $\mu\text{m}$ , i.e. the particle size is much larger than the wavelength. Therefore, the scattering in our experiment is the Mie scattering. In the Mie regime, with the stated refractive index, most of the energy is forward-scattered at each particle [46], which justifies the chosen propagation model that is in effect a single scattering model that discards the reflection of light backward at each particle.

If significantly smaller particles or longer wavelengths were to be used, one would have to replace the model with a significantly more complex bidirectional propagation (see e.g. [47]).

## 4 PHYSICS-BASED HOLOGRAPHIC PARTICLE IMAGING VELOCIMETRY

Flow fields and particles are coupled with each other. Different frame particles are driven by the flow velocity field. In our work, we consider the flow velocity field and particle field reconstructions as joint reconstructions so that we can have more information and more constraints for both unknowns. Aggregating temporal information coupled with physical constraints improves the particle positions, which in turn improves the flow estimates.

This work focuses on the study of incompressible fluids, a common situation in many turbulent fluid analyses. Our approach involves starting with the Navier-Stokes equation and then incorporating the incompressible constraint as a prior in the optimization problem. In the end, we arrive at the following optimization model:

$$\begin{aligned} (\mathbf{v}^*, \mathbf{n}^*) = \arg \min_{\mathbf{v}, \mathbf{n}} & \sum_{t=1}^T \|\hat{\mathbf{I}}_t(\mathbf{n}_t) - \mathbf{I}_t\|_2^2 + \kappa_0 \sum_{t=1}^T \|\mathbf{n}_t\|_1 + \\ & \kappa_1 \sum_{t=1}^{T-1} \|\nabla_t \mathbf{n}_t + \nabla_s \mathbf{n}_t \cdot \mathbf{v}_t\|_2^2 + \kappa_2 \sum_{t=1}^{T-1} \|\nabla \mathbf{v}_t\|_2^2 \\ \text{s.t. } & \mathbf{v}_t = \Pi_{C_{DIV}}(\mathbf{v}_t) \quad \mathbf{n}_t = \Pi_{[0,1]}(\mathbf{n}_t) \end{aligned} \quad (9)$$

$\mathbf{n} = [\mathbf{n}_1, \mathbf{n}_2, \dots, \mathbf{n}_T]^t$  is the refractive index for  $T$  frames.  $\mathbf{v} = [\mathbf{v}_1, \mathbf{v}_2, \dots, \mathbf{v}_{T-1}]'$  is the flow velocity field for  $T-1$  frames.  $\hat{\mathbf{I}}_t(\cdot)$  is the forward process that we described in Section 3.  $t$  is the frame number,  $\kappa$  the loss weight, while  $\nabla_t$  and  $\nabla_s$  respectively refer to the temporal and spatial derivatives.  $\Pi_{C_{DIV}}$  refers to a divergence-free projection, which will be described in Section 4.2.1. To solve this problem, we will split it into two subproblems: one is particle volume reconstruction and the other is velocity field reconstruction. We use an alternative optimization framework to solve this problem. In the following sections, we will describe them in detail.

### 4.1 Particle Volume Reconstruction

The first subproblem is to optimize for refractive index  $\mathbf{n}$  representing the particle distribution in the volume. Therefore, we assume the other unknown velocity field  $\mathbf{v}$  is a constant during this step. Then the Eq. 9 becomes:

$$\begin{aligned} \mathbf{n}^* = \arg \min_{\mathbf{n}} & \sum_{t=1}^T \|\hat{\mathbf{I}}_t(\mathbf{n}_t) - \mathbf{I}_t\|_2^2 + \kappa_0 \sum_{t=1}^T \|\mathbf{n}_t\|_1 + \\ & \kappa_1 \sum_{t=1}^{T-1} \|\mathbf{n}_{t+1} - \Omega_{\mathbf{v}_t} \mathbf{n}_t\|_2^2 \\ \text{s.t. } & \mathbf{n}_t = \Pi_{[0,1]}(\mathbf{n}_t) \end{aligned} \quad (10)$$

Here,  $\Omega_{\mathbf{v}_t}$  refers to a volume warp operation that warps an existing particle field using the velocity field  $\mathbf{v}_t$ . The third term in Eq. 10 is the particle motion consistency term, which is necessary to account for the temporal coherence and continuity present in real flows. This term ensures that the particle volume at time  $t$ , warped by the velocity field  $\mathbf{v}_t = (u_t, v_t, k_t)$ , aligns with the subsequent frame. By enforcing temporal coherence, it enhances particle position

estimation once the velocity field is estimated and integrates the reconstruction of all frames into a single optimization problem.  $\Pi_{[0,1]}$  refers to the projection of element to the interval  $[0, 1]$ , which is a convex operator.

#### 4.1.1 Automatic Differentiation

We solve this optimization problem by using gradient descent with step size  $\tau$  ( $\mathcal{L}$  refers to the optimization term from Eq. 10):

$$\mathbf{n}^{n+1} = \mathbf{n}^n - \tau \nabla \mathcal{L}(\mathbf{n}^n) \quad (11)$$

To efficiently and accurately compute gradients  $\nabla \mathcal{L}$ , we leverage automatic differentiation in PyTorch, which uses the chain rule to trace derivative information through complex calculations. For example, by chain rule, for Eq. 10, we have:

$$\frac{\partial \mathcal{L}}{\partial \mathbf{n}} = \frac{\partial f_1}{\partial \mathbf{n}} + \kappa_0 \frac{\partial f_2}{\partial \mathbf{n}} + \kappa_1 \frac{\partial f_3}{\partial \mathbf{n}} = \frac{\partial \hat{\mathbf{I}}^T}{\partial \mathbf{n}} \cdot \frac{\partial f_1}{\partial \hat{\mathbf{I}}} + \kappa_0 \frac{\partial f_2}{\partial \mathbf{n}} + \kappa_1 \frac{\partial f_3}{\partial \mathbf{n}}, \quad (12)$$

where  $f_1 = \sum_{t=1}^T \|\hat{\mathbf{I}}_t(\mathbf{n}_t) - \mathbf{I}_t\|_2^2$ ,  $f_2 = \sum_{t=1}^T \|\mathbf{n}_t\|_1$  and  $f_3 = \sum_{t=1}^{T-1} \|\mathbf{n}_{t+1} - \Omega_{\mathbf{v}_t} \mathbf{n}_t\|_2^2$ .

For  $f_1$ , if we want to find the gradient, we need to trace derivatives back to the light field of every slice, which leads to expressions Eq. 5 and Eq. 8. Note that Eq. 5 describes a complex-valued function of complex variables. For such functions to be differentiable everywhere, they have to be *holomorphic*, which is not the case here. However, we can introduce the Wirtinger derivatives [48] so that even if the function is not holomorphic, we can still get the gradient and do gradient descent. The Wirtinger derivatives of a complex variable and its complex conjugate are defined as

$$\begin{aligned} \frac{\partial}{\partial \mathbf{U}_k} &= \frac{1}{2} \left( \frac{\partial}{\partial \Re[\mathbf{U}_k]} - j \frac{\partial}{\partial \Im[\mathbf{U}_k]} \right) \\ \frac{\partial}{\partial \bar{\mathbf{U}}_k} &= \frac{1}{2} \left( \frac{\partial}{\partial \Re[\mathbf{U}_k]} + j \frac{\partial}{\partial \Im[\mathbf{U}_k]} \right) \end{aligned} \quad (13)$$

Using the corresponding chain rule [48] on the optimization term  $\mathcal{L}$  from Eq. 5, we get:

$$\frac{\partial \mathcal{L}}{\partial \bar{\mathbf{U}}_{k-1}} = \frac{\partial \mathcal{L}}{\partial \mathbf{U}_k} \frac{\partial \mathbf{U}_k}{\partial \bar{\mathbf{U}}_{k-1}} + \frac{\partial \mathcal{L}}{\partial \bar{\mathbf{U}}_k} \frac{\partial \bar{\mathbf{U}}_k}{\partial \bar{\mathbf{U}}_{k-1}} \quad (14)$$

We know that  $\frac{\partial \mathcal{L}}{\partial \mathbf{U}_k} = \overline{\frac{\partial \mathcal{L}}{\partial \bar{\mathbf{U}}_k}}$ , while  $\frac{\partial \mathbf{U}_k}{\partial \bar{\mathbf{U}}_{k-1}}$  and  $\frac{\partial \bar{\mathbf{U}}_k}{\partial \bar{\mathbf{U}}_{k-1}}$  can be obtained from combining the Wirtinger derivative Eq. 13 and Eq. 5.

## 4.2 Velocity Field Reconstruction

In our work, we focused on studying an incompressible fluid, which is a common scenario in fluid imaging. Therefore, we add this incompressibility assumption as a physical prior to the flow reconstruction. It is a very strong prior, which decreases uncertainty in the flow solution. In this section, we introduce the incompressible physical prior and its implementation known as pressure projection.

### 4.2.1 Incompressibility

A classical result from fluid mechanics is that incompressible flows are *divergence free* or *solenoidal*, with  $\mathbf{v} = \mathbf{v}_{\text{sol}}$  and

$$\nabla \cdot \mathbf{v}_{\text{sol}} = 0 \quad (15)$$

This property can be used as a prior in fluid reconstruction tasks [33], [49]. The Helmholtz decomposition provides a powerful framework for analyzing general vector fields and deriving such a prior. Specifically, the Helmholtz decomposition allows us to decompose an arbitrary vector field  $\mathbf{v}$  into its solenoidal (divergence-free) and irrotational (curl-free) components. Furthermore, any curl-free vector field can be interpreted as the gradient of a scalar field, in our case  $\mathcal{P}/\rho$  where  $\mathcal{P}$  is the scalar pressure field, and  $\rho$  is the scalar mass density field [33]. Therefore, the Helmholtz decomposition can be expressed as:

$$\mathbf{v} = \mathbf{v}_{\text{sol}} + \nabla \mathcal{P}/\rho \quad (16)$$

From the vector identities,  $\mathbf{v}_{\text{sol}}$  and  $\nabla \mathcal{P}/\rho$  are orthogonal subspaces [49], meaning that we obtain the closest incompressible (solenoidal) flow  $v_{\text{sol}}$  to an arbitrary input velocity field  $v$  by subtracting the curl-free component. This curl-free component can in turn be calculated by taking the divergence of both sides of Eq. 16, yielding

$$\begin{aligned} \nabla \cdot \mathbf{v} &= \nabla \cdot \mathbf{v}_{\text{sol}} + \nabla^2 \mathcal{P}/\rho \\ &= \nabla^2 \mathcal{P}/\rho \end{aligned} \quad (17)$$

Eq 17 indicates that the curl-free field  $\mathcal{P}/\rho$ , also known as the *pressure gradient* can be obtained from the original flow field by solving a Poisson equation. The pressure gradient is then subtracted from the original flow to yield the incompressible (solenoidal) flow. It is worth noting that this projection of  $v$  onto  $v_{\text{sol}}$  is a projection  $\Pi_{\mathcal{C}_{DIV}}$  onto a convex set, and can therefore be interpreted as a proximal operator [49]:

$$\mathbf{v}_{\text{sol}} = \Pi_{\mathcal{C}_{DIV}}(\mathbf{v}) = \mathbf{v} - \nabla \mathcal{P}/\rho \quad (18)$$

### 4.2.2 Optimization

Incorporating the above derivation as a physics-based prior, we aim to reconstruct the flow velocity field by incorporating the incompressible physical prior. This serves as an alternating optimization step within Equation (9), with the particle volume  $\mathbf{n}$  treated as a constant. The optimization problem can be formulated as follows:

$$\begin{aligned} \mathbf{v}^* = F = \arg \min_{\mathbf{v}} \kappa_1 \sum_{t=1}^{T-1} & \|\nabla_t \mathbf{n}_t + \nabla_s \mathbf{n}_t \cdot \mathbf{v}_t\|_2^2 \\ & + \kappa_2 \sum_{t=1}^{T-1} \|\nabla \mathbf{v}_t\|_2^2 \\ \text{s.t. } \mathbf{v}_t &= H = \Pi_{\mathcal{C}_{DIV}}(\mathbf{v}_t) \end{aligned} \quad (19)$$

Eq. 19 can be considered a variant of the Horn-Schunck optical flow model [50]. The term  $\|\nabla \mathbf{v}_t\|_2^2$  enforces smoothness and sparsity in the flow field changes. The problem can be treated as a constraint optimization problem and

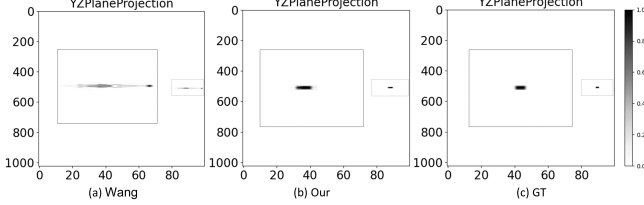


Fig. 2. One particle reconstruction result comparison (a) Wang method reconstruction result (b) Our method of reconstruction results (c) Synthetic particle ground truth

transformed into an augmented Lagrangian function. We solve it using the ADMM (Alternating Direction Method of Multipliers) framework.

#### Algorithm 1 ADMM Framework of Computing Fluid Velocity Vector Fields

```

1: procedure OPTICALFLOWDIVFREE( $F, H$ )
2:   for from 1 to ADMM iterations do
3:      $v_t^{n+1} \leftarrow prox_{\sigma_1 F}(z^n - q^n)$      $\triangleright u$  optimization
4:      $z^{n+1} \leftarrow prox_{\tau_1 H}(v^{n+1} + q^n)$      $\triangleright z$  optimization
5:      $q^{n+1} \leftarrow q + v_t^{n+1} - z^{j+1}$      $\triangleright$  scaled dual variables
       update
6:   end for
7: end procedure

```

The  $F$  proximal operator is just the Horn-Schunck optical flow problem. For the detailed derivation of this proximal operator, please refer to the supplement. means projecting a velocity field into divergence-free space. The projection is implemented by Eq. (17) and Eq. (18). To deal with large displacements, we build a coarse-to-fine pyramid architecture. We first did a Gaussian blur and made a pyramid of different scales of volumes. Then, we begin computing the flow with the coarse volume. This result will be the initial value for the next level optical flow field.

## 5 EXPERIMENTS

In this section, we present the results of our experiments using both synthetic and real experimental data. Specifically, we conducted some ablation studies to examine the impact of particle density, tank depth, frame number, and a plane-to-plane model on the reconstruction performance of our proposed method. Our findings demonstrate the significance of employing the plane-to-plane model to account for the scattering effect and the resultant improvement in reconstruction performance due to the inclusion of the physical prior. The metrics we use to evaluate the reconstruction quality are the average angular error (AAE) [51] and the average endpoint error (EPE) [52]. Detailed discussion and expressions for AAE and EPE can be found in the supplement.

### 5.1 Synthetic Data

#### 5.1.1 Particle Reconstruction Result

In this section, we conducted a simulation using synthetic data. First, we generated particles with a diameter of approximately 40  $\mu\text{m}$ . Subsequently, we generated a rotation

flow using the formula described in the supplement Section 4.2. Based on this flow, we calculated the particle position transformation to obtain the next frame particle volume. It is important to acknowledge that acquiring a "ground truth" scattering light field for multiple particles on a large scale is a challenging task. The FDTD can get an accurate result, but for this physical scale, the FDTD is infeasible. As mentioned in Section 2 and Section 3 the BPM is considered accurate enough based on the Mie scattering regime in the relatively sparse volume density of particles. Therefore, we employ BPM simulation as the "ground truth" hologram to evaluate different reconstruction methods.

Figure 2 shows one particle reconstruction result. The 3D volume was projected onto the YZ plane, and the value was averaged along the x direction. We place a zoom-in patch beside the reconstructed particle for better observation. Figure 2a, referred to as the Wang method [25], a long tail is observed, indicating uncertainty regarding the particle position. This is associated with single-camera reconstruction. Single-camera settings result in information being lost about the particle shape and a missing part in the frequency domain (the missing cone problem [53]). On the other hand, our method in Figure 2b incorporates additional physical priors and utilizes multiple measurements, resulting in a more accurate and robust particle reconstruction. Notably, our approach effectively addresses the issue of particle elongation, leading to improved depth accuracy. Finally, Figure 2c shows the synthetic particle ground truth, which is very close to our reconstruction result. These results demonstrate the effectiveness of our method in accurately reconstructing particle shape and position.

The results of the multiple particle reconstruction are presented in Fig. 3. We generated 50 particles and reconstructed them using a voxel scale of  $1.38 \times 1.38 \times 30 \mu\text{m}$  and a reconstruction grid size of  $128 \times 128 \times 100$ . Our method is observed to produce sharper reconstruction results than Wang's method [25]. "w/o Flow+DIV" refers to our particle reconstruction method without adding the particle motion consistency and divergence-free physics prior. "w Flow+DIV" means our full method with all priors. It can be observed that the particle motion consistency constraint and divergence-free physics prior significantly improves the reconstruction quality and mitigate the elongation problem, as evidenced by the sharper reconstructed particle shapes in Fig. 3b-c. Additionally, it is worth noting that better flow reconstruction can also improve particle reconstruction results. Our reconstructed particles are observed to be very close to the ground truth.

#### 5.1.2 Flow Reconstruction Result

To quantitatively evaluate the performance of our algorithm on real-world flows, we conducted experiments on the Johns Hopkins Turbulence Database (JHUTDB) [54], which contains high-resolution measurements of turbulence in various configurations. Specifically, we tested our algorithm on a flow from the Forced Isotropic Turbulence configuration, as shown in Fig. 4. The reconstruction volume consisted of  $128 \times 128 \times 100$  voxels with a physical scale of  $27.6 \times 27.6 \times 50 \mu\text{m}$ , and we simulated 500 particles in the flow.

Our reconstruction results for this realistic flow are also very good, as evidenced by an AAE of 13.83 and EPE of

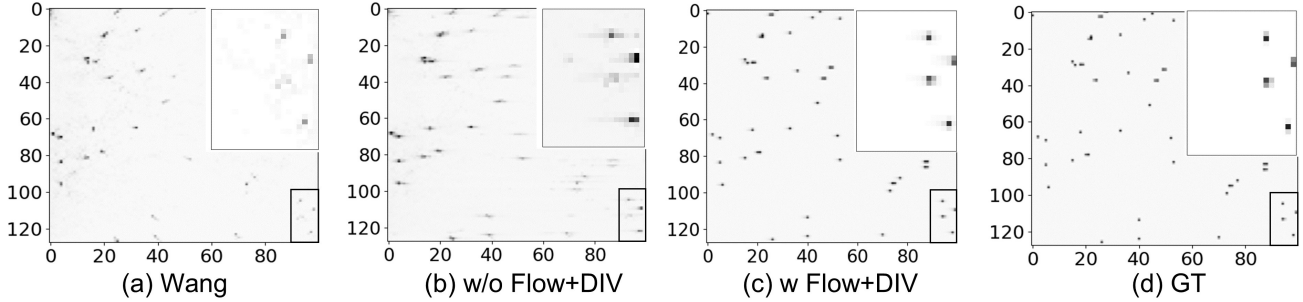


Fig. 3. Multiple particle reconstruction result comparison. (a) Wang method reconstruction result (b) Our particle reconstruction method without adding particle motion consistency and incompressible prior (d) Our method reconstruction results with particle motion consistency and incompressible prior (d) Synthetic particle ground truth

0.3648. The detail of the flow can be recovered very well. More synthetic flow reconstruction results are provided in the supplementary materials.

## 5.2 Ablation Study

**Particle Density and Tank Depth Impact** This section presents an ablation study to investigate the influence of different particle densities and tank depths on the PIV reconstruction results. The results are summarized in Table 1, where the AAE and EPE values are reported. The symbol '-' indicates reconstruction failure. ppp means particle per pixel, i.e. it refers to the 2D density of the particles in the image plane, which is a common metric to evaluate the particle density in PIV experiments. As expected, a declining trend occurs in reconstruction accuracy with an increasing tank depth and particle density. However, the proposed method exhibits promising results for a wide range of particle densities. Additionally, the proposed method has better performance and can achieve some reconstruction depth that Wang's method [25] cannot.

**Plane2Plane and OnePlane2Last** We conducted an ablation study to investigate the influence of plane-to-plane propagation on PIV reconstruction for different particle densities because a denser particle can recover more detail of the fluid flow. Therefore, particle density is a crucial factor. However, denser particles also lead to more significant scattering effects. To address this issue, the plane-to-plane propagation approach was introduced. This approach accounts for the interaction of scattering light across different planes, enabling it to consider the scattering effect. In comparison, most HPIV methods use the one-plane-to-last approach, which does not consider the interaction between planes. Therefore, we conducted this ablation study to investigate the influence of the scattering effect on the PIV reconstruction process and evaluate how our plane-to-plane model can improve the results. In comparison, most HPIV methods use the one-plane-to-last approach, which does not consider the interaction between planes inside the volume. To evaluate the effectiveness of the plane-to-plane model, we conducted a comparison study with the one-plane-to-last method, where the light field of each slice is propagated directly to the camera plane with the angular spectrum

propagation kernel  $\mathbf{H}'$ . The hologram is obtained by summing the propagated field of each slice. Unlike the plane-to-plane propagation approach, there is no interaction between different planes inside the volume with this method. In the experiment, we varied the particle density from 0.006 to 0.04 and used two models for the reconstruction. Two frames ( $T = 2$ ) with a voxel number of  $256 \times 256 \times 100$  were used, and the ground-truth flow was from isotropic 4096 in the JHTDB. The center of the reconstructed particle was computed and compared with the ground-truth particle center. The results are shown in Fig. 5, where the first row displays the plane-to-plane reconstruction result and the second row displays the one-plane-to-last reconstruction result. As the particle density increases, the number of wrong reconstructions (red dots) and missing reconstructions (green dots) increases for both methods. However, the plane-to-plane reconstruction has fewer red and green dots compared to the one-plane-to-last method. Furthermore, we computed the AAE value for the reconstructed flow velocity field at different particle densities for both models, as presented in Fig. 4 in the supplement. The plane-to-plane model achieved better AAE values for almost all particle densities, demonstrating its effectiveness in accounting for the scattering effect. In conclusion, this ablation study demonstrates that the scattering phenomenon cannot be overlooked in high-density particle PIV reconstruction. The proposed plane-to-plane model provides a better result for higher-density PIV reconstruction by accounting for the scattering effect.

**Number of frames** We conducted an ablation study to investigate the influence of the number of frames on the PIV reconstruction results. Longer sequences can provide more temporal information that can be aggregated to improve both the velocities and the particle densities. To demonstrate this effect, we conducted an experiment using 2 measurement frames ( $T = 2$ ) and 5 measurement frames ( $T = 5$ ) for velocity field reconstruction. We generated different particle densities varying from 0.02 to 0.3. The reconstruction voxel number is  $128 \times 128 \times 100$ . The ground-truth flow is isotropic 1024fine from JHTDB. We did reconstruction by using 2 frames and 5 frames at different particle densities.

We computed the AAE for two frames and five frames of velocity field reconstruction under different particle densities. The AAE results are provided in Fig. 6.

From Fig. 6, the five frames reconstruction has a better AAE value than the two frames reconstruction results.

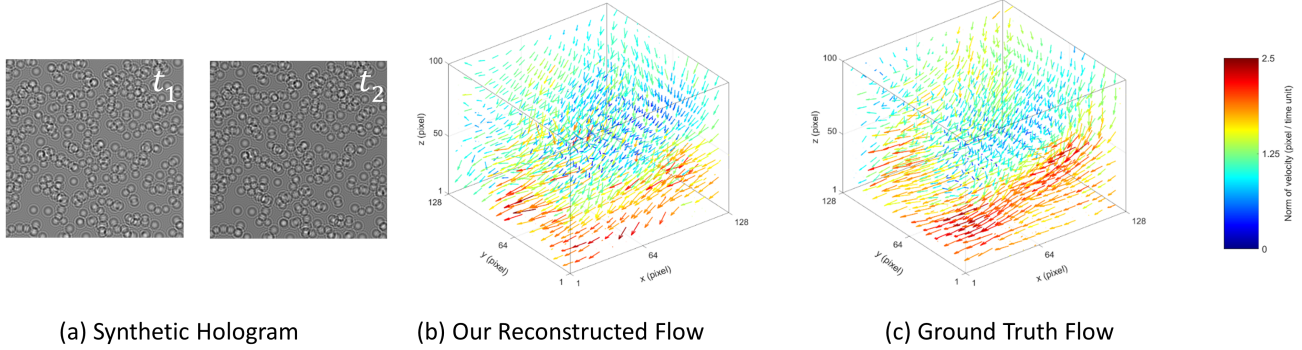


Fig. 4. The turbulent flow reconstruction result (a) Synthetic particle hologram frames (b) Our reconstructed flow result (c) Ground truth flow

TABLE 1  
The Quantitative evaluation (AAE in degree / EPE in voxel) of different particle densities at different tank depth.

Particle Density(ppp)	Tank depth(mm)					
	1	2	3	4	5	
0.002	Wang(AAE/EPE) Our(AAE/EPE)	15.42/0.3788 9.68/0.2537	19.37/0.6211 10.32/0.2648	22.66/0.9113 9.82/0.2583	- 13.24/0.3318	- 14.63/0.3592
0.004	Wang(AAE/EPE) Our(AAE/EPE)	16.58/0.3974 9.23/0.2439	19.21/0.5922 10.67/0.2685	23.46/0.8972 9.97/0.2677	21.84/0.9827 12.98/0.3197	- 13.26/0.3418
0.006	Wang(AAE/EPE) Our(AAE/EPE)	16.75/0.4176 10.33/0.2862	19.48/0.6812 11.47/0.2981	22.13/0.9615 10.59/0.3022	- 12.69/0.3135	- 14.18/0.3413
0.008	Wang(AAE/EPE) Our(AAE/EPE)	16.82/0.3886 11.83/0.3071	19.24/0.5463 11.23/0.2877	23.03/1.1614 11.42/0.2861	- 13.46/0.3382	- 15.13/0.3674

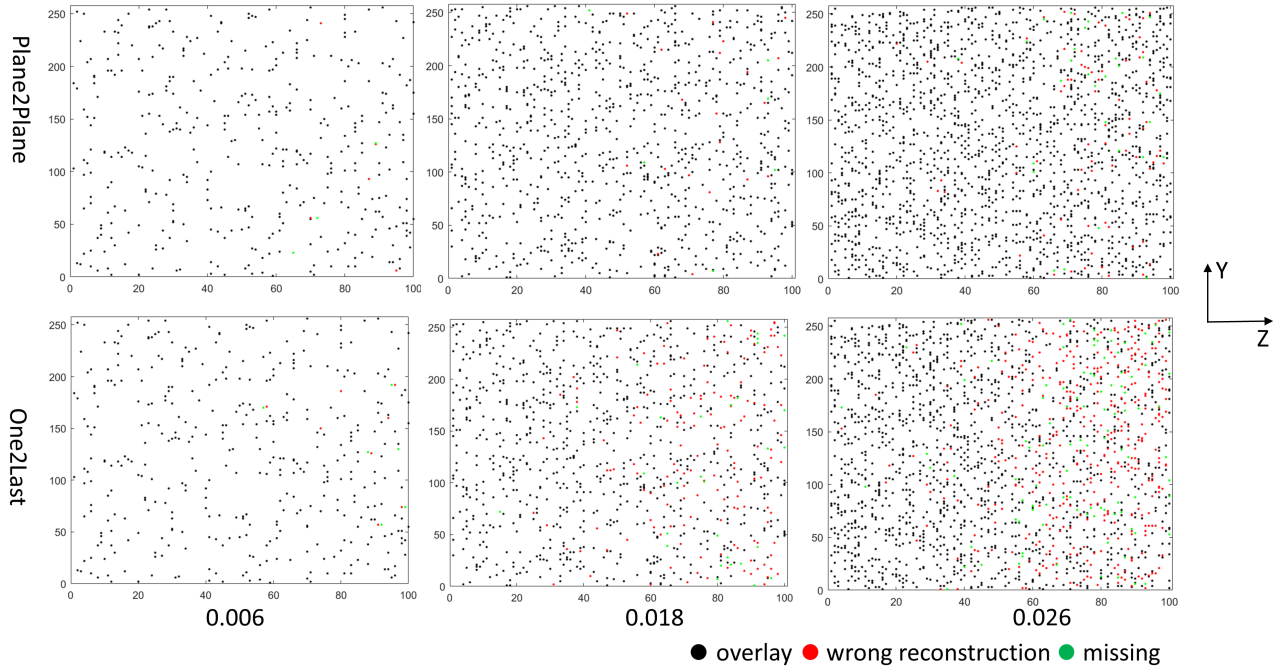


Fig. 5. Plane-to-plane model vs. the one-plane-to-last model. The center of the reconstructed particle is computed and compared with the ground-truth particle center. All the images are in the YZ projection plane.

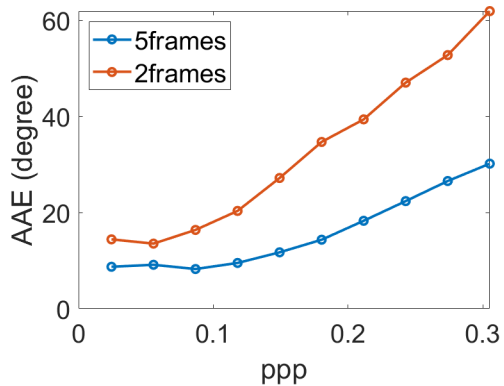


Fig. 6. Reconstruction AAE as a function of particle density (particles per pixel). We show reconstructions from two frames and five frames. Reconstruction quality degrades with increasing density, and the degradation is substantially slower for five-frame sequences because these can aggregate more temporal information with the physical motion priors.

Moreover, employing more frames enables us to achieve a density of 0.3 particles per pixel with good accuracy.

To further analyze the reconstruction accuracy, we computed the reconstructed flow velocity field error by subtracting the reconstructed velocity field from the ground-truth velocity field. The error magnitude results are presented in Fig. 7, where red indicates higher errors and blue indicates smaller errors. As expected, the five-frame reconstruction has a lower error than the two-frames reconstruction, indicating that more frames provide more information for the reconstruction, yielding more accurate results. In conclusion,

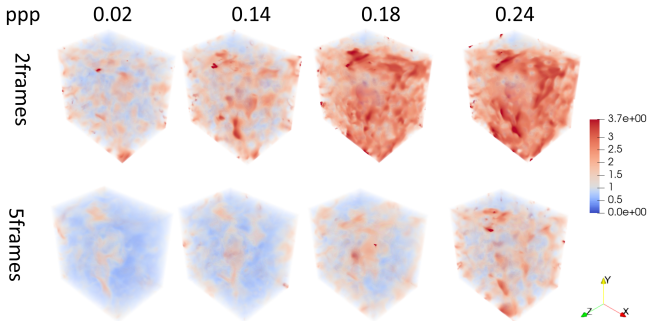


Fig. 7. Error magnitude for two frames and five frames flow velocity reconstruction. Five-frame reconstruction presents the velocity field between the first and the second frames.

the experiment demonstrates that increasing the number of measurement frames improves the accuracy of PIV reconstruction. The results reveal that using more frames can lead to a higher particle density and a more accurate velocity field reconstruction, which is beneficial for applications that require high-fidelity flow information.

### 5.3 Real Experiments

#### 5.3.1 Experiment with Ground Truth

We evaluated the performance on the captured hologram of real flows. For a quantitative assessment of the flow, we

filled a tank with a high-viscosity liquid, so that the particle positions are frozen in place. The particle size is about 40  $\mu\text{m}$ . We placed the tank in the translation stage (Thorlabs XYT1/M), which moves in a direction (the  $x$  direction) that is perpendicular to the optical axis. The setup description and figure are in the supplement Section 3, 4.4 and Fig. 5. Two holograms are obtained at a distance of 49.993  $\mu\text{m}$ . Thus, we created a shifting flow with a known distance, which is the ground truth. The reconstruction results are presented in Fig. 8. The reconstructed flow reveals that the reconstructed flow is a shifting flow in the  $x$  direction.

In addition, we can perform a quantitative analysis of the reconstructed results by comparing them to ground-truth movements. This allows us to evaluate the accuracy of the reconstruction. The ground-truth movement is 49.993  $\mu\text{m}$  by controlling the translation stage. The reconstruction result shows that the mean of the movement is 42.18653  $\mu\text{m}$ , with a standard derivation of 9.61  $\mu\text{m}$ . The experimental results demonstrate a high degree of agreement with the theoretical values, indicating that the reconstruction is very accurate.

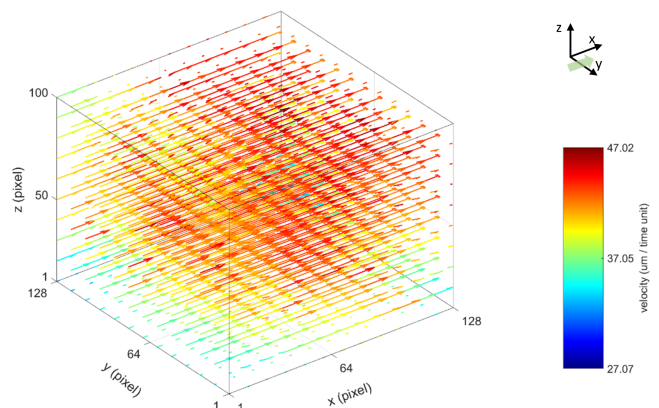


Fig. 8. The reconstructed velocity vector fields from the hologram frames induced by moving the particle volume with a translation stage

#### 5.3.2 Experiment Without Ground Truth

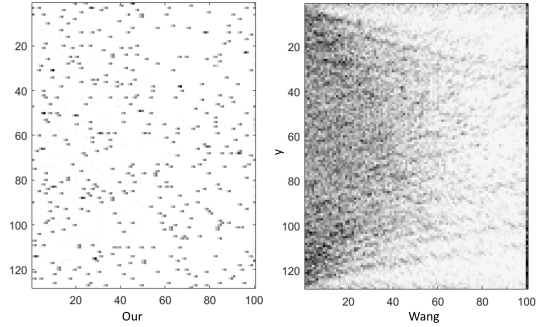


Fig. 9. The particle reconstruction comparison between our method and Wang's method for real experiment.

We also tested the proposed method for real turbulent flow in the experimental setup described in the supplementary material Section 3. The shutter speed is 0.036 ms and the frame rate is about 10 fps. We downsampled the holograms with a factor of 16, from  $2048 \times 2048$  to  $128 \times 128$ .

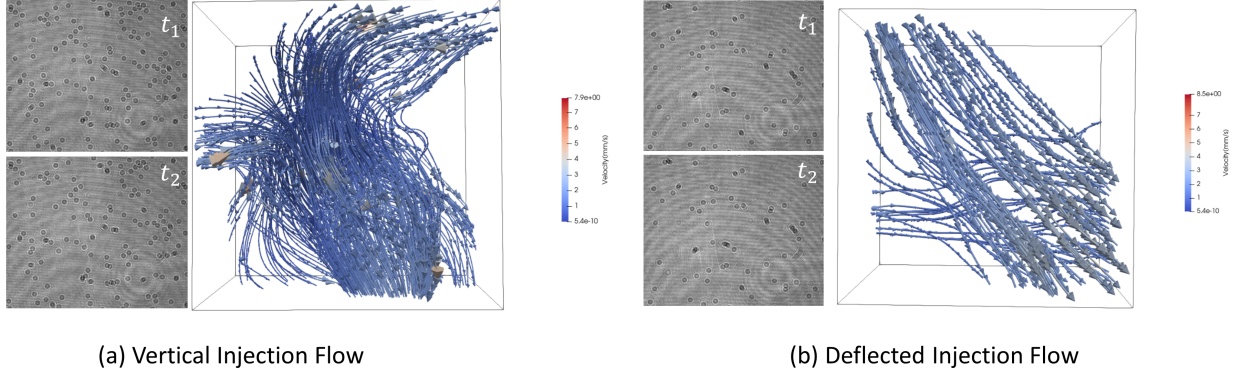


Fig. 10. Jet flow reconstruction: (a) vertical injection flow reconstruction streamline (b) deflected injection flow reconstruction streamline

The reconstruction grid resolution is  $128 \times 128 \times 100$  with voxel sizes  $55.2 \times 55.2 \times 50 \mu\text{m}$ . To create a jet flow, we used a syringe to inject fluid in a specific direction, which we then varied. The particle reconstruction result is shown in Fig. 9. The left is our reconstruction result. The right is Wang's method [25]. In this 5mm tank depth and ppp 0.01 density, Wang's method will fail. Our method can still reconstruct the particles and flow. Our flow reconstruction results are presented in Fig. 10. In Fig. 10(a), we present a streamlined visualization of the vertical injection flow reconstruction result. This figure clearly shows the presence of converging flows from both the left and right sides that merge into a single downward stream. Fig. 10 (b) displays the reconstruction result of a deflected injection flow. We can see the mainstream is deflected compared to Fig. 10(a). By conducting this experiment, we demonstrated the capability of the proposed method to effectively reconstruct real turbulent flows in experimental setups and help the application of turbulence analysis.

## 6 DISCUSSION AND CONCLUSION

We introduced a novel HPIV reconstruction method. This method enables the reconstruction of particles and the flow velocity field with a single camera and a very simple setup. To account for the effect of light scattering in our study, we developed a plane-to-plane beam propagation method model. This approach allowed us to accurately model the propagation of light through a scattering medium by dividing the medium into thin slices and simulating the interaction of light between each slice. Except for this plane-to-plane propagation, we combined the particle and flow reconstruction into a joint optimization problem, which improves both the particle reconstruction and flow estimation. Moreover, to improve the reconstruction result, we also incorporated the motion consistency prior and underlying physical incompressible prior into the optimization. Again, this improves both the flow estimation and the particle reconstruction. We introduced an AD and alternative optimization framework to solve this joint optimization problem.

We verified the proposed method in the synthetic flow and real jet flow. Both have good performance and are better than the previous method. We conducted ablation studies to demonstrate the necessity of a plane-to-plane model

for high-density HPIV reconstruction. And also, conducted ablation studies show that with our physical priors and multiple frame measurements, we can improve the reconstruction accuracy and push particle density and tank depth to higher levels.

However, the potential limitation of the proposed approach is that the reconstruction will take a very long time. This can be attributed to the utilization of a first-order optimization method. We think that a good initialization may help with speeding up the convergence, like the spectral initialization mentioned in the paper [55]. The other reason is the H&S optical flow optimization problem. It may take a long time, especially for high-resolution reconstruction. This limits the large-scale reconstruction application. One possible way is to solve the 3D optical flow using some of the most advanced deep learning methods. This may improve the result and save a lot of time.

Despite these limitations, our proposed approach demonstrates a way to take the light scattering effect into consideration when developing the holographic particle imaging velocity system. Our system setup is simple, and reconstruction accuracy is good. It can be used to investigate some real turbulence flow in fluid dynamics. Besides, our framework can also be transferred to some other space-time scattering theory model, like the Mie scattering model or the optical diffraction tomography model [43].

## ACKNOWLEDGMENTS

The authors would like to thank Ni Chen who has contributed to the idea and implementation of framework, but does not take responsibility for other aspects and the paper writing. The author thank Congli Wang, Jinhui Xiong and Yuanhao Wang for their discussion and help. Sigurdur Thoroddsen, Ziqiang Yang, Andres A. Aguirre-Pablo and Abdullah Alhareeth from High-Speed Fluids Imaging Laboratory at KAUST provided help with the preparation of the particles, and design the flow experiments. This work was supported by KAUST individual baseline funding.

## REFERENCES

- [1] R. J. Adrian and J. Westerweel, *Particle image velocimetry*. Cambridge university press, 2011, no. 30.
- [2] M. Raffel, C. E. Willert, J. Kompenhans *et al.*, *Particle image velocimetry: a practical guide*. Springer, 1998, vol. 2.

- [3] J. Xiong and W. Heidrich, "In-the-wild single camera 3d reconstruction through moving water surfaces," in *Proceedings of the IEEE/CVF International Conference on Computer Vision*, 2021, pp. 12558–12567.
- [4] J. Du, G. Zang, B. Mohan, R. Idoughi, J. Sim, T. Fang, P. Wonka, W. Heidrich, and W. L. Roberts, "Study of spray structure from non-flash to flash boiling conditions with space-time tomography," *Proceedings of the Combustion Institute*, vol. 38, no. 2, pp. 3223–3231, 2021.
- [5] J. Gu, S. K. Nayar, E. Grinspun, P. N. Belhumeur, and R. Ramamoorthi, "Compressive structured light for recovering inhomogeneous participating media," *IEEE transactions on pattern analysis and machine intelligence*, vol. 35, no. 3, pp. 1–1, 2012.
- [6] T. Hawkins, P. Einarsson, and P. Debevec, "Acquisition of time-varying participating media," *ACM Transactions on Graphics (ToG)*, vol. 24, no. 3, pp. 812–815, 2005.
- [7] S. W. Hasinoff and K. N. Kutulakos, "Photo-consistent reconstruction of semitransparent scenes by density-sheet decomposition," *IEEE transactions on pattern analysis and machine intelligence*, vol. 29, no. 5, pp. 870–885, 2007.
- [8] I. Ihrke and M. Magnor, "Image-based tomographic reconstruction of flames," in *Proceedings of the 2004 ACM SIGGRAPH/Eurographics symposium on Computer animation*, 2004, pp. 365–373.
- [9] K. Okamoto, S. Nishio, T. Saga, and T. Kobayashi, "Standard images for particle-image velocimetry," *Measurement Science and Technology*, vol. 11, no. 6, p. 685, 2000.
- [10] C. Brücker, "3d scanning piv applied to an air flow in a motored engine using digital high-speed video," *Measurement Science and Technology*, vol. 8, no. 12, p. 1480, 1997.
- [11] T. Hori and J. Sakakibara, "High-speed scanning stereoscopic piv for 3d vorticity measurement in liquids," *Measurement Science and Technology*, vol. 15, no. 6, p. 1067, 2004.
- [12] A. K. Prasad, "Stereoscopic particle image velocimetry," *Experiments in fluids*, vol. 29, no. 2, pp. 103–116, 2000.
- [13] Y. Wang, R. Idoughi, and W. Heidrich, "Stereo event-based particle tracking velocimetry for 3d fluid flow reconstruction," in *Computer Vision–ECCV 2020: 16th European Conference, Glasgow, UK, August 23–28, 2020, Proceedings, Part XXIX 16*. Springer, 2020, pp. 36–53.
- [14] G. E. Elsinga, F. Scarano, B. Wieneke, and B. W. van Oudheusden, "Tomographic particle image velocimetry," *Experiments in fluids*, vol. 41, no. 6, pp. 933–947, 2006.
- [15] J. Trolinger, R. Belz, and W. Farmer, "Holographic techniques for the study of dynamic particle fields," *Applied Optics*, vol. 8, no. 5, pp. 957–961, 1969.
- [16] N. Chen, Y. Li, and W. Heidrich, "Physics-based holo-net for three-dimensional imaging," in *3D Image Acquisition and Display: Technology, Perception and Applications*. Optica Publishing Group, 2020, pp. JTH3D–3.
- [17] N. Chen, C. Wang, and W. Heidrich, "Holographic 3d particle imaging with model-based deep network," *IEEE Transactions on Computational Imaging*, vol. 7, pp. 288–296, 2021.
- [18] D. J. Brady, K. Choi, D. L. Marks, R. Horisaki, and S. Lim, "Compressive holography," *Optics express*, vol. 17, no. 15, pp. 13 040–13 049, 2009.
- [19] K. Mallery and J. Hong, "Regularized inverse holographic volume reconstruction for 3d particle tracking," *Optics Express*, vol. 27, no. 13, pp. 18 069–18 084, 2019.
- [20] W. Tahir, U. S. Kamilov, and L. Tian, "Holographic particle localization under multiple scattering," *Advanced Photonics*, vol. 1, no. 3, pp. 036 003–036 003, 2019.
- [21] U. S. Kamilov, I. N. Papadopoulos, M. H. Shoreh, A. Goy, C. Vonesch, M. Unser, and D. Psaltis, "Optical tomographic image reconstruction based on beam propagation and sparse regularization," *IEEE Transactions on Computational Imaging*, vol. 2, no. 1, pp. 59–70, 2016.
- [22] S. BEA and M. Teich, "Fundamentals of photonics," Wiley, p. 313, 1991.
- [23] M. S. Wartak, *Computational photonics: an introduction with MATLAB*. Cambridge University Press, 2013.
- [24] S. Chowdhury, M. Chen, R. Eckert, D. Ren, F. Wu, N. Repina, and L. Waller, "High-resolution 3d refractive index microscopy of multiple-scattering samples from intensity images," *Optica*, vol. 6, no. 9, pp. 1211–1219, 2019.
- [25] H. Wang, W. Tahir, J. Zhu, and L. Tian, "Large-scale holographic particle 3d imaging with the beam propagation model," *arXiv preprint arXiv:2103.05808*, 2021.
- [26] L. Tian and L. Waller, "3d intensity and phase imaging from light field measurements in an led array microscope," *optica*, vol. 2, no. 2, pp. 104–111, 2015.
- [27] C. Wang, N. Chen, and W. Heidrich, "do: A differentiable engine for deep lens design of computational imaging systems," *IEEE Transactions on Computational Imaging*, vol. 8, pp. 905–916, 2022.
- [28] F. Pereira, M. Gharib, D. Dabiri, and D. Modarress, "Defocusing digital particle image velocimetry: a 3-component 3-dimensional dpiv measurement technique. application to bubbly flows," *Experiments in fluids*, vol. 29, no. Suppl 1, pp. S078–S084, 2000.
- [29] F. Pereira and M. Gharib, "Defocusing digital particle image velocimetry and the three-dimensional characterization of two-phase flows," *Measurement Science and Technology*, vol. 13, no. 5, p. 683, 2002.
- [30] S. Y. Yoon and K. C. Kim, "3d particle position and 3d velocity field measurement in a microvolume via the defocusing concept," *Measurement Science and Technology*, vol. 17, no. 11, p. 2897, 2006.
- [31] J. Belden, T. T. Truscott, M. C. Axiak, and A. H. Techet, "Three-dimensional synthetic aperture particle image velocimetry," *Measurement Science and Technology*, vol. 21, no. 12, p. 125403, 2010.
- [32] F. Scarano, "Tomographic piv: principles and practice," *Measurement Science and Technology*, vol. 24, no. 1, p. 012001, 2012.
- [33] J. Xiong, R. Idoughi, A. A. Aguirre-Pablo, A. B. Aljedaani, X. Dun, Q. Fu, S. T. Thoroddsen, and W. Heidrich, "Rainbow particle imaging velocimetry for dense 3d fluid velocity imaging," *ACM Transactions on Graphics (TOG)*, vol. 36, no. 4, pp. 1–14, 2017.
- [34] A. Aguirre-Pablo, A. B. Aljedaani, J. Xiong, R. Idoughi, W. Heidrich, and S. T. Thoroddsen, "Single-camera 3d ptv using particle intensities and structured light," *Experiments in Fluids*, vol. 60, pp. 1–13, 2019.
- [35] Y. Ding, Z. Li, Z. Chen, Y. Ji, J. Yu, and J. Ye, "Full-volume 3d fluid flow reconstruction with light field piv," *IEEE Transactions on Pattern Analysis and Machine Intelligence*, 2023.
- [36] Z. Li, Y. Ji, J. Yu, and J. Ye, "3d fluid flow reconstruction using compact light field piv," in *Computer Vision–ECCV 2020: 16th European Conference, Glasgow, UK, August 23–28, 2020, Proceedings, Part XVI 16*. Springer, 2020, pp. 120–136.
- [37] J. Xiong, A. A. Aguirre-Pablo, R. Idoughi, S. T. Thoroddsen, and W. Heidrich, "Rainbowpiv with improved depth resolution—design and comparative study with tomopiv," *Measurement Science and Technology*, vol. 32, no. 2, p. 025401, 2020.
- [38] N. Chen, C. Wang, and W. Heidrich, "Compact computational holographic display," *Frontiers in Photonics*, vol. 3, p. 5, 2022.
- [39] ———, "∂ h: Differentiable holography," *Laser & Photonics Reviews*, 2023. doi: 10.1002/lpor.202200828 Accepted for publication.
- [40] ———, "Snapshot space-time holographic 3d particle tracking velocimetry," *Laser & Photonics Reviews*, vol. 15, no. 8, p. 2100008, 2021.
- [41] E. Wolf, "Three-dimensional structure determination of semi-transparent objects from holographic data," *Optics communications*, vol. 1, no. 4, pp. 153–156, 1969.
- [42] A. Devaney, "Inverse-scattering theory within the rylov approximation," *Optics letters*, vol. 6, no. 8, pp. 374–376, 1981.
- [43] H.-Y. Liu, D. Liu, H. Mansour, P. T. Boufounos, L. Waller, and U. S. Kamilov, "Seagle: Sparsity-driven image reconstruction under multiple scattering," *IEEE Transactions on Computational Imaging*, vol. 4, no. 1, pp. 73–86, 2017.
- [44] E. Soubies, T.-A. Pham, and M. Unser, "Efficient inversion of multiple-scattering model for optical diffraction tomography," *Optics express*, vol. 25, no. 18, pp. 21 786–21 800, 2017.
- [45] K. Matsushima and T. Shimobaba, "Band-limited angular spectrum method for numerical simulation of free-space propagation in far and near fields," *Optics express*, vol. 17, no. 22, pp. 19 662–19 673, 2009.
- [46] C. F. Bohren and D. R. Huffman, *Absorption and scattering of light by small particles*. John Wiley & Sons, 2008.
- [47] P. L. Ho and Y. Y. Lu, "A bidirectional beam propagation method for periodic waveguides," *IEEE Photonics technology letters*, vol. 14, no. 3, pp. 325–327, 2002.
- [48] C. Boeddeker, P. Hanebrink, L. Drude, J. Heymann, and R. Haeb-Umbach, "On the computation of complex-valued gradients with application to statistically optimum beamforming," *arXiv preprint arXiv:1701.00392*, 2017.
- [49] J. Gregson, I. Ihrke, N. Thuerey, and W. Heidrich, "From capture to simulation: connecting forward and inverse problems in fluids," *ACM Transactions on Graphics (TOG)*, vol. 33, no. 4, pp. 1–11, 2014.

- [50] B. K. Horn and B. G. Schunck, "Determining optical flow," *Artificial intelligence*, vol. 17, no. 1-3, pp. 185–203, 1981.
- [51] J. L. Barron, D. J. Fleet, and S. S. Beauchemin, "Performance of optical flow techniques," *International journal of computer vision*, vol. 12, pp. 43–77, 1994.
- [52] M. Otte and H. H. Nagel, "Optical flow estimation: advances and comparisons," in *Computer Vision—ECCV'94: Third European Conference on Computer Vision Stockholm, Sweden, May 2–6, 1994 Proceedings, Volume I 3*. Springer, 1994, pp. 49–60.
- [53] J. Lim, K. Lee, K. H. Jin, S. Shin, S. Lee, Y. Park, and J. C. Ye, "Comparative study of iterative reconstruction algorithms for missing cone problems in optical diffraction tomography," *Optics express*, vol. 23, no. 13, pp. 16 933–16 948, 2015.
- [54] Y. Li, E. Perlman, M. Wan, Y. Yang, C. Meneveau, R. Burns, S. Chen, A. Szalay, and G. Eyink, "A public turbulence database cluster and applications to study lagrangian evolution of velocity increments in turbulence," *Journal of Turbulence*, no. 9, p. N31, 2008.
- [55] E. J. Candes, X. Li, and M. Soltanolkotabi, "Phase retrieval via wirtinger flow: Theory and algorithms," *IEEE Transactions on Information Theory*, vol. 61, no. 4, pp. 1985–2007, 2015.

**Miao Qi** is a Ph.D. student in the Visual Computing Center at King Abdullah University of Science and Technology. He received his M.S degree in electrical engineering at Peking University in 2018. His research interests are computational imaging and deep learning.



**Wolfgang Heidrich** (Fellow, IEEE) is a Professor of Computer Science and Electrical and Computer Engineering in the KAUST Visual Computing Center, for which he also served as director from 2014 to 2021. Heidrich joined KAUST in 2014, after 13 years as a faculty member at the University of British Columbia. He received his PhD in from the University of Erlangen in 1999, and then worked as a Research Associate in the Computer Graphics Group of the Max-Planck-Institute for Computer Science

in Saarbrücken, Germany, before joining UBC in 2000. Heidrich's research interests lie at the intersection of imaging, optics, computer vision, computer graphics, and inverse problems. His more recent interest is in computational imaging, focusing on hardware-software co-design of the next generation of imaging systems, with applications such as High-Dynamic Range imaging, compact computational cameras, hyperspectral cameras, to name just a few. His work on HDR displays serves as the basis for many modern-day HDR consumer devices today. Heidrich is a Fellow of the IEEE, AAIA, and Eurographics, and the recipient of a Humboldt Research Award as well as the ACM SIGGRAPH Computer Graphics Achievement Award.

